Measuring interactions between tunnel-coupled quantum dots

F. R. Waugh,* M. J. Berry,† C. H. Crouch, C. Livermore, D. J. Mar,‡ and R. M. Westervelt
Division of Applied Sciences and Department of Physics, Harvard University, Cambridge, Massachusetts 02138

K. L. Campman and A. C. Gossard
Materials Department, University of California, Santa Barbara, California 93106
(Received 30 June 1995; revised manuscript received 25 September 1995)

We report low-temperature tunneling measurements through double and triple quantum dots with adjustable interdot tunnel conductance, fabricated in a GaAs/$Al_xGa_{1-x}As$ heterostructure. As interdot tunnel conductance is increased, Coulomb blockade conductance peaks split into two peaks for double dots and three for triple dots. The splitting approaches zero for weak tunneling and saturates as the dots merge for strong tunneling. Coupled double and triple dots with different gate capacitance show quasiperiodic beating and peak suppression for weak interdot tunneling. Analysis of the data in terms of tunneling and classical charging theories shows that quantum charge fluctuations due to interdot tunneling dominate dot interactions when interdot tunnel conductance approaches $2e^2/h$.

I. INTRODUCTION

Quantum dots are often described as artificial atoms and as single-electron transistors.[1–4] Both labels imply their use as building blocks in larger structures. In the first case, quantum-dot arrays may form custom-engineered artificial molecules or artificial crystals.[5–14] These differ from their real counterparts in that leads may be attached and conductance spectroscopy performed as gates tune their size, shape, electron number, or coupling. In the second case, quantum-dot arrays may form logic circuits in which individual electrons represent bits of information.[3,4,15–17] Arrays of submicron metal islands already demonstrate useful computing functions.[18,19]

An understanding of interactions between quantum dots is crucial to these uses of dot arrays. The many phenomena predicted for interacting dots,[20–31] which include conductance peak splitting, miniband formation, quasiperiodic peak suppression, and single-electron solitons, can be difficult to observe without experimental control over interdot coupling. However, many array architectures do not allow such control: couplings between metal islands or between vertical semiconductor dots are fixed in fabrication,[18,19] and couplings between lateral semiconductor dots are often not independently tunable because a single modulated gate defines the dot array.[5,6,11]

In this paper, we extend a previous study[12,13] of interdot tunneling in two- and three-dot arrays defined in a two-dimensional electron gas by tunable gates. The device architecture permits separate control of tunnel barriers and confining walls, allowing compensation for impurity-induced disorder and also enabling the interdot tunnel conductance $G_{\rm int}$ to be varied. We find that interdot tunneling leads to a variety of phenomena not observed for single dots. Opening the interdot quantum point contacts leads to a continuous transition from isolated dots to one large dot as $G_{\rm int}\rightarrow 2e^2/h$. Isolated dot arrays show strong Coulomb blockade conductance peaks vs gate voltage, which split into two peaks for double dots and three peaks for triple dots as the tunnel conductance increases. The splitting approaches zero for weak tunneling, $G_{\rm int}\ll 2e^2/h$, and saturates as the dots merge for strong tunneling, $G_{\rm int}\rightarrow 2e^2/h$, consistent with recent theories of tunnel-coupled dots.[30,31] For dot arrays with unequal gate capacitances, conductance peaks exhibit beating, quasiperiodicity and peak suppression for weak interdot tunneling. While our observations for *weakly* coupled dots are consistent with classical capacitive charging,[1–4,7,20,22,23] we show that peak splitting for *strongly* coupled dots is a quantum phenomenon arising from interdot tunneling. Such tunneling interactions have been predicted for coupled dots[27–31] and also for single dots coupled to their leads,[32–35] but they have not been reported in other recent coupled dot experiments.[7–10]

Models of interacting quantum dots are summarized in Sec. II. Section III describes sample fabrication and measurement. Section IV characterizes the point contacts and individual dots that form the arrays. Double-dot and triple-dot experimental data are presented in Secs. V and VI, respectively, and are compared to predictions of quantum tunneling and classical charging theories. Section VII summarizes our results.

II. MODELS OF COUPLED QUANTUM DOTS

Peak splitting in tunnel-coupled dot arrays can be understood[12,30,31] by starting with single-dot capacitive charging models.[1–4] Consider two or three identical dots weakly tunnel coupled to external leads, so that the total number of electrons $N_{\rm tot}=\Sigma N_i$ is a good quantum number, where N_i is the number of electrons on dot i. If interdot tunneling is also weak, then the N_i for each dot are also good quantum numbers and the ''orthodox'' theory of single electron charging[1–4] applies: the energy of a single dot is the charging energy

$$U_i=\frac{(eN_i-C_gV_g)^2}{2C_\Sigma} \tag{1}$$

plus the sum over single-particle states E_n. In Eq. (1), C_g, V_g, and C_Σ are the gate capacitance, gate voltage, and total capacitance, assumed to be the same for all dots.

We first consider dot arrays with negligible interdot tunnel conductance and negligible interdot capacitance. In keeping with our experiments, we take $E_F>U>\Delta E>k_BT$, with E_F the Fermi energy, $U=e^2/C_\Sigma$ the charging energy, and $\Delta E\cong 2E_F/N$ the average level spacing. At these low temperatures, the ground state for each dot charge configuration $(N_1N_2\ldots)$ dominates equilibrium transport. In the absence of dot interactions, the ground-state energy is simply the sum of the single-dot charging energies U_i from Eq. (1), minimized over all charge configurations. Charge configurations with no internal polarization, meaning that the N_i are the same for all dots, have the lowest energy; polarized configurations with different N_i on some or all dots have higher energy and do not participate in transport.[12] Thus the array conductance vs gate voltage V_g is qualitatively similar to that of a single dot, with conductance peaks occurring when all N_i simultaneously change by 1.[12]

When interdot tunnel conductance is no longer negligible, quantum charge fluctuations between dots can destroy polarization, allowing polarized configurations to decrease in energy and participate in transport. As shown in Ref. 12, a decrease Δ in the energy of a polarized configuration leads to conductance peak splitting

$$\Delta V_s=\frac{2C_\Sigma}{C_ge}\Delta. \tag{2}$$

For strong tunneling, peak splitting must physically saturate when the dots merge into one. At saturation, the decrease in ground-state energy reaches its maximum value, $\Delta_{\max}=e^2/4C_\Sigma$ for double dots and $\Delta_{\max}=e^2/3C_\Sigma$ for triple dots. A useful quantity is the fractional peak splitting F, which compares ΔV_s to the peak separation $\Delta V_p=e/C_g$ in the absence of splitting, and is defined so that $0\leqslant F\leqslant 1$:

$$F=\frac{\Delta}{\Delta_{\max}}=\begin{cases}\dfrac{2\Delta V_s}{\Delta V_p} & \text{(double dots)}\\[2ex] \dfrac{3\Delta V_s}{2\Delta V_p} & \text{(triple dots).}\end{cases} \tag{3}$$

The quantities ΔV_s and ΔV_p are shown in Fig. 5(b) for double dots.

Peak splitting due to interdot tunneling has been studied theoretically using a variety of approaches. Hubbard model calculations[27–29] for vertical dots with many tunneling modes and with $\Delta E\sim e^2/C_\Sigma$ predict a peak splitting proportional to an interdot tunneling matrix element t; they fail to capture the splitting saturation for strong tunneling. More recently, many-body calculations[30,31] have been performed for coupled dots with few tunneling modes and with $\Delta E\ll e^2/C_\Sigma$, as in our experiments. The peak splitting is found to be a universal function $F(G_{\rm int})$ of the interdot tunnel conductance $G_{\rm int}$ that saturates exactly at $F(2e^2/h)=1$ for tunnel barriers with two modes. The splitting is proportional to $G_{\rm int}$ for weak tunneling, $G_{\rm int}\ll 2e^2/h$, and has a logarithmic form for strong tunneling, $G_{\rm int}\to 2e^2/h$. We show in Sec. V that these recent theories agree well with our experiments, which have two interdot tunneling modes and $\Delta E\cong 0.1e^2/C_\Sigma$.

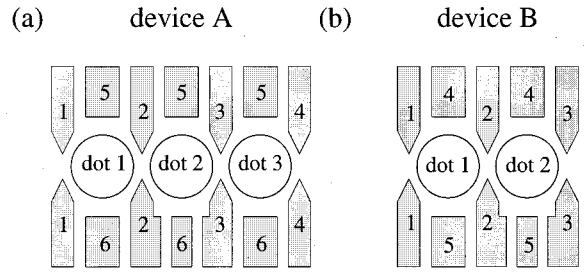

FIG. 1. Schematic diagrams of (a) triple dot (device A) and (b) double dot (device B). Dots are formed in a GaAs/Al_xGa_{1-x}As heterostructure, and have a lithographic area 0.5×0.8 μm^2.

Classical interdot capacitance also reduces the energy of polarized charge configurations and leads to conductance peak splitting.[22,23] A purely capacitive description of the observed peak splitting, however, requires that interdot capacitance increase strongly while interdot tunnel conductance remains negligible. We show in Secs. V and VI that our experiments fulfill neither of these requirements. Nevertheless, other interesting phenomena are associated with capacitive charging in dot arrays. Unequal gate capacitance can lead to conductance peak suppression through the stochastic Coulomb blockade.[7,22,23,30] For double quantum dots, peak suppression results from quasiperiodic beating between periods $\sim e/C_{g1}$ and $\sim e/C_{g2}$, leading to peak amplitude modulation with period $\sim e/|C_{g1}-C_{g2}|$, where C_{g1} and C_{g2} are the gate capacitances for dots 1 and 2. A similar beating occurs for more than two dots. With increased interdot tunnel conductance, peak suppression is lifted and peaks split through the same mechanism described above.[30]

III. DEVICE FABRICATION AND MEASUREMENT

We studied two devices: a triple dot (device A), used also for double-dot experiments by not energizing all gates; and a similar double dot (device B). Schematic diagrams of both devices appear in Fig. 1, and a scanning electron micrograph of device A appears as Fig. 1(a) of Ref. 12. Both devices were fabricated using the same GaAs/A1$_x$Ga$_{1-x}$As heterostructure, which contains a two-dimensional electron gas located 470 Å beneath the surface with sheet density $n_s=3.7\times 10^{11}$ cm^{-2}, mobility $\mu=5\times 10^5$ cm^2/V s at $T=10$ K, and a phase coherence length >20 μm for $T<1$ K.[36]

Device A consists of 14 Schottky gates fabricated on the heterostructure surface with electron-beam lithography and chrome/gold evaporation. As shown in Fig. 1(a), eight gates form the four quantum point contacts used as tunnel barriers, and six gates form the dot confining walls, when sufficient negative voltage is applied to deplete the electron gas underneath. The lithographic area of each dot is $A_{\rm dot}=0.5\times 0.8$ μm^2. The number of electrons per dot is considerably less than $n_sA_{\rm dot}=1500$, because depletion extends beyond the gates and because the electron density is reduced throughout

the dots. The device is wired with six independently tunable gate voltages: one for each tunnel barrier (V_1 through V_4) and one for each set of confining walls at the top (V_5) and bottom (V_6) of the array; note that the confining wall for dot 2 on gate 6 is intentionally made smaller than the others. Double-dot experiments were conducted using device *A* by not energizing V_1. Device *B*, shown schematically in Fig. 1(b), is similar to device *A* but consists of ten Schottky gates forming two coupled quantum dots, also with area $A_{\rm dot}=0.5\times0.8\ \mu{\rm m}^2$.

The samples were cooled in a He dilution refrigerator at the base mixing chamber temperature $T_{\rm mc}=14$ mK. Care was taken to shield them from external electromagnetic radiation, which can induce photon-assisted tunneling through conductance channels that are otherwise energetically forbidden.[37,38] The electromagnetic shielding of our dilution refrigerator is discussed in Ref. 38. The differential conductance of quantum point contacts, single dots, and tunnel-coupled dot arrays was measured at the base temperature with no dc source-drain bias by applying a small (typically 5–10 μV) ac voltage at 11 Hz and recording the current with a current preamplifier and lock-in amplifier. In addition, the differential conductance of single dots was measured (i) at temperatures between the base and 400 mK with no dc source-drain bias, and (ii) at base temperature with dc source-drain biases up to 500 μV in magnitude.

IV. QUANTUM POINT CONTACTS AND SINGLE QUANTUM DOTS

An important advantage of our quantum-dot arrays is that each component is controlled by separate gates and can be individually tested and adjusted. This section describes measurements characterizing the quantum point contacts, gates, and single dots that make up the arrays.

Tunability is particularly important for the quantum point contacts used as tunnel barriers, because it permits compensation for disorder arising from the impurity potential.[39,40] As shown in Fig. 2(a), the four nominally identical quantum point contacts of device *A*, separately measured, each show high-quality characteristics $G_{\rm qpc}$ vs gate voltage with up to five quantized conductance plateaus and with pinchoff voltages ranging from -0.92 to -1.02 V. The three quantum point contacts of device *B* also show high-quality characteristics, plotted in Fig. 2(b), with up to six plateaus and with pinchoff voltages from -0.77 to -0.82 V. For both devices the spread in pinchoff voltages demonstrates the need for independent gate tunability, as it is not possible to bias all point contacts in the tunneling regime using a single gate voltage.

The total capacitance and single-particle level spacing were measured for a single dot by applying a dc source-drain bias $V_{\rm bias}$ to dot 1 of device *A*. Figure 3(a) plots the location of conductance peaks in the plane of $V_{\rm bias}$ and gate voltage V_5, clearly showing rhombus-shaped regions of Coulomb blockade.[1–4,41] The vertical extent of these regions experimentally determines the single-dot total capacitance $C_\Sigma\cong360$ aF and charging energy $U=e^2/C_\Sigma\cong440\ \mu$eV. Figure 3(b) shows the single-dot differential conductance $dI/dV_{\rm bias}$ vs $V_{\rm bias}$ for the value of V_5 corresponding to the vertical dashed line in Fig. 3(a). Additional peaks in Fig. 3(b) outside the Coulomb blockade region arise from single-particle levels with separation $\Delta E\cong50\ \mu$eV.

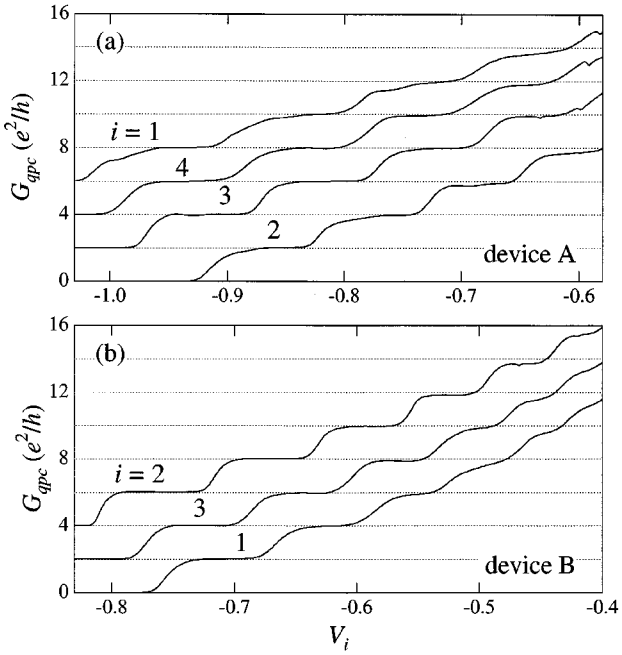

FIG. 2. (a) For device *A*, four quantum point contact characteristics G_{qpc} vs their respective gate voltages V_i, $i=1,\ldots,4$, labeled as in Fig. 1(a). (b) For device *B*, three quantum point contact characteristics $G_{\rm qpc}$ vs their respective gate voltages V_i, $i=1,\ldots,3$, labeled as in Fig. 1(b). The spread in pinchoff voltages demonstrates the need for independent tunability. In (a) and (b), each characteristic is measured with all other gates grounded, and each curve is offset by $2e^2/h$ from the curve below.

The temperature dependence of conductance peak amplitudes and widths also provides information about dot energy scales. Figure 4(a) shows the zero-bias single-dot conductance $G_{\rm sd}$ vs gate voltage V_5 for dot 1 of device *A*, measured at four mixing chamber temperatures $T_{\rm mc}$ from 40 to 400 mK. Figure 4(b) shows the amplitude (left axis) and width (right axis) of a single peak of Fig. 4(a) vs $T_{\rm mc}$. The peak width ΔV_5, determined from fits to a thermally broadened line shape,[1–4,41,42] has been converted to an electron temperature T using the relation $k_BT=eC_{35}\Delta V_5/2C_\Sigma$, where $C_{35}=41$ aF is the measured capacitance between dot 3 and gate 5 (see below). There are two important features of Fig. 4(b). First, the sharp increase in peak amplitude as $T_{\rm mc}$ decreases indicates that at each conductance peak electrons tunnel through a single dot state, implying that $k_BT<\Delta E$.[42] Second, T decreases to well below 100 mK at the lowest $T_{\rm mc}$, so that $k_BT\cong7\,\mu$eV.

The separation in gate voltage ΔV_p between adjacent conductance peaks determines the capacitance $C_{ia}=e/\Delta V_p$ between dot i and gate a.[1–4] Measurements similar to Fig. 4(a) were made at the base temperature for all three dots of device *A* using gates 5 and 6, and for both dots of device *B* using gates 4 and 5. For device *A*, the gate capacitances are $C_{15}=38$ aF, $C_{25}=43$ aF, $C_{35}=41$aF, $C_{16}=41$ aF, $C_{26}=32$ aF, and $C_{36}=39$ aF. For device *B*, the gate capacitances are $C_{14}=43$ aF, $C_{24}=42$ aF, $C_{15}=44$ aF, and $C_{25}=25$ aF.

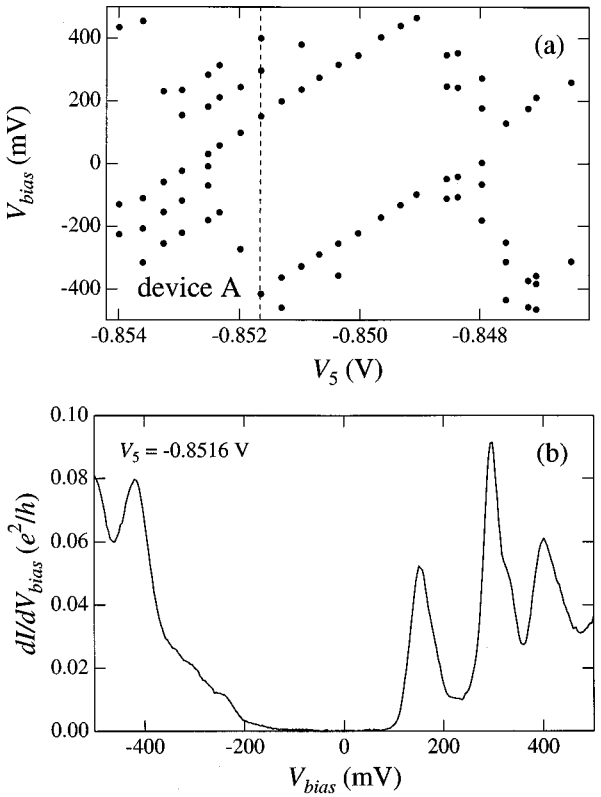

FIG. 3. (a) Location of conductance peaks in the plane of bias voltage $V_{\rm bias}$ and gate voltage V_5 for dot 1 of device A. The height of the rhombus-shaped Coulomb blockade regions determines the total capacitance $C_\Sigma \cong 360$ aF and charging energy $U = e^2/C_\Sigma \cong 400$ μeV. (b) Single-dot differential conductance $dI/dV_{\rm bias}$ vs $V_{\rm bias}$ for $V_5 = -0.8516$ V, corresponding to the vertical dashed line in (a). Peaks outside the Coulomb blockade region arise from single-particle levels with separation $\Delta E \cong 50$ μeV.

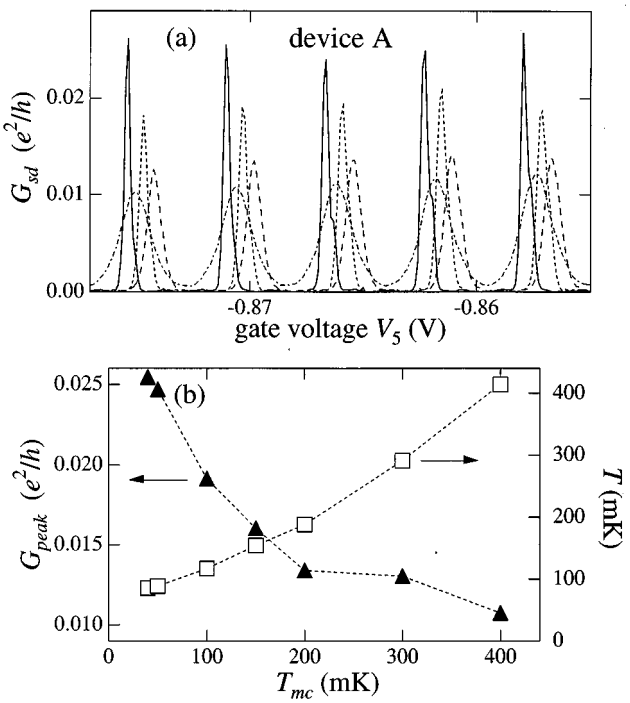

FIG. 4. (a) Single-dot conductance $G_{\rm sd}$ vs gate voltage V_5 for dot 1 of device A for mixing chamber temperatures $T_{\rm mc} = 40$ mK (solid), 100 mK (short dash), 200 mk (long dash), and 400 mK (dot-dash). (b) For the peak at $V_5 = -0.871$ V in (a), peak amplitude $G_{\rm peak}$ (triangles, left axis) and peak width (squares, right axis) vs mixing chamber temperature $T_{\rm mc}$. Peak width ΔV_5 is converted to electron temperature T using $k_B T = eC_{35}\Delta V_5/2C_\Sigma$. Dashed lines are guides.

V. DOUBLE QUANTUM DOTS

This section describes experiments on double dots that show how interdot tunneling leads to conductance peak splitting. The experiments determine the dot interaction energy Δ due to tunneling, as well as the relationship $F(G_{\rm int})$ between peak splitting F, defined in Eq. (3), and interdot tunnel barrier conductance $G_{\rm int}$. For unequal gate capacitances, peak amplitude and splitting show quasiperiodic beating due to the stochastic Coulomb blockade.[7,22,23,30]

Figures 5(a)–5(d) show changes in the conductance $G_{\rm dd}$ of a double dot vs gate voltage with increasing interdot tunnel conductance $G_{\rm int}$. The double dot is formed in device B by energizing all gates; gate voltage V_4 is swept, and gate voltage V_2 controls $G_{\rm int}$. In Fig. 5(a), interdot tunneling is weak. The double-dot conductance consists of weakly split peaks, with the same average separation ΔV_p in gate voltage that appears in Fig. 4(a) for single dots. Each conductance peak in Fig. 5(a) corresponds to adding two electrons to the double dot, one to each dot. In Figs. 5(b) and 5(c), each peak clearly splits into two peaks whose separation increases with interdot tunnel conductance. Finally, in Fig. 5(d), the tunnel barrier between dots 2 and 3 is removed, and the conductance is that of a single large dot with a peak separation half that in Fig. 5(a). A similar peak splitting with increased interdot tunnel conductance is seen in double dots formed with device A, and appears as Fig. 2 of Ref. 12. While uncontrolled peak splitting attributed to disorder has been observed in dots and metal islands,[43–45] Ref. 12 was, to our knowledge, the first observation of peak splitting controlled via tunable gates.

Recent calculations[30,31] predict a universal relationship $F(G_{\rm int})$ between peak splitting and tunnel conductance for tunnel-coupled dots with few tunneling modes and with an energy-level spacing less than the charging energy $\Delta E \ll e^2/C_\Sigma$. Remarkably, the theory predicts that the splitting saturates exactly at $F(2e^2/h) = 1$ for dots coupled by two tunneling modes. In addition, the calculations predict functional forms for $F(G_{\rm int})$ in the weak- and strong-tunneling limits:

$$F(G_{\rm int}) = \frac{4\ln 2}{\pi^2}\frac{hG_{\rm int}}{2e^2} \quad (\text{weak tunneling, } G_{\rm int} \ll 2e^2/h), \tag{4}$$

$$F(G_{\rm int}) = 1 + \frac{16e^\gamma}{\pi^3}\left(1 - \frac{hG_{\rm int}}{2e^2}\right)\ln\left(1 - \frac{hG_{\rm int}}{2e^2}\right)$$

$$(\text{strong tunneling, } G_{\rm int} \to 2e^2/h), \tag{5}$$

where $\gamma \cong 0.577$ in Eq. (5).

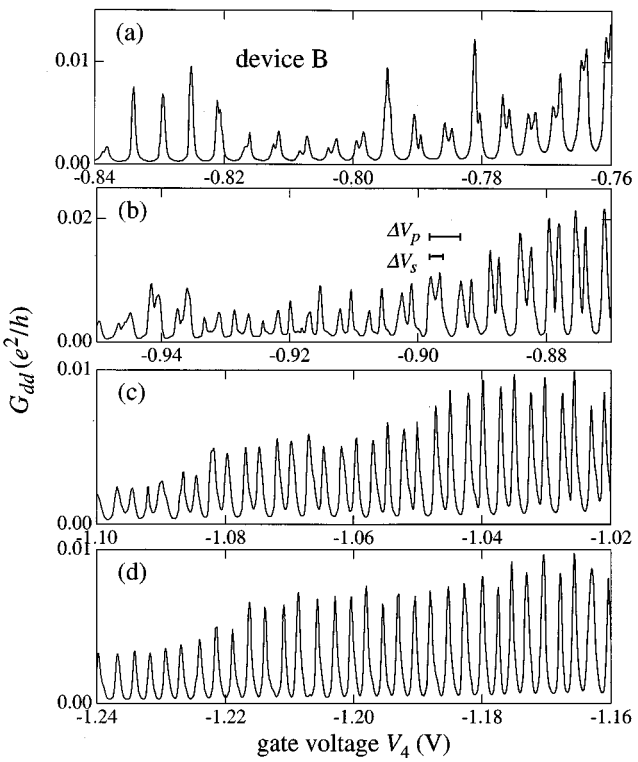

FIG. 5. For device B, double-dot conductance $G_{\rm dd}$ vs gate voltage V_4 as the interdot tunnel conductance increases from (a) to (d). Tunneling splits the conductance peaks, with split peak separation ΔV_s proportional to the interaction energy Δ [Eq. (2)]. Gate voltage V_2 controlling interdot tunnel barrier 2 is (a) -0.770 V, (b) -0.760 V, (c) -0.750 V, and (d) -0.700 V. The double dot of device A shows a similar behavior, reported in Fig. 2 of Ref. 12.

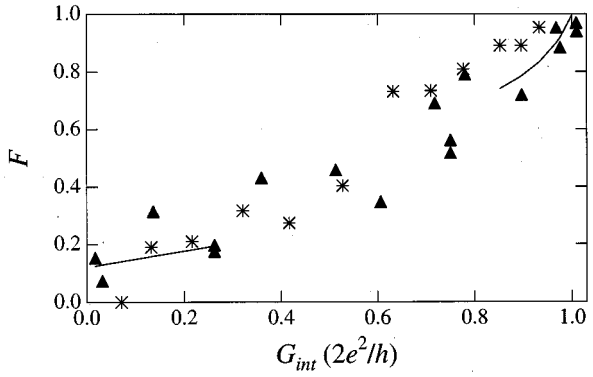

FIG. 6. Fractional peak splitting F [Eq. (3)] plotted vs the tunnel barrier conductance $G_{\rm int}$ for the double dot of device A. Triangles and asterisks are data from Figs. 3(a) and 3(b) of Ref. 12, respectively. Curves are theoretically predicted forms of $F(G_{\rm int})$, Eqs. (4) and (5), for weak and strong tunneling (Refs. 31 and 32); the only adjustable parameter is the weak-tunneling intercept $F(G_{\rm int}=0)$, which accounts for interdot capacitance $G_{\rm int}\cong 20$ aF.

Figure 6 plots the experimentally measured relationship between F and $G_{\rm int}$ for double dots formed in device A by grounding gate 1 and energizing all other gates, so that gate voltage V_3 controls $G_{\rm int}$. Each triangle represents the average value of F over different sweeps of gate voltage V_5, with V_3 changed between sweeps; each asterisk represents the value of F in a single sweep of gate voltage V_3, with V_5 held constant (see Fig. 3 of Ref. 12). Values of $G_{\rm int}$ are determined by horizontally shifting the separately measured tunnel barrier conductance from Fig. 2(a) by 70 mV to account for the influence of other gates.[12] As predicted by the theory, the observed splitting plotted in Fig. 6 approaches zero for weak tunneling and saturates for strong tunneling. Also displayed in Fig. 6 are the limiting forms of Eqs. (4) and (5). The universal theory has no adjustable parameters, but we have added a small offset in F at $G_{\rm int}=0$ to account for an interdot capacitance of $C_{\rm int}\cong 20$ aF.[14,30] This value is consistent with the measured gate capacitances $C_g\sim 40$ aF. A careful analysis of the slopes of the rhombus edges in Coulomb blockade data similar to Fig. 3(a) for coupled dots in device A also yields $C_{\rm int}\cong 20$ aF.[14] Using Eq. (3) with the measured value $C_\Sigma\cong 360$ aF implies that Δ ranges from 0 to 110 μeV in the transition from weak to strong tunneling.

Numerical simulations[13] of a classical charging model[20,22,23] also give peak splittings qualitatively similar to experiment. However, several features of the simulations are inconsistent with our experiments. Classical charging models assume that electrons are point charges, dots hold integer numbers of electrons, and tunneling is a sequential Markov process whose rate is determined by the electrostatic energy difference before and after tunneling occurs. In these models, the capacitance $C_{\rm int}$ between dots determines the dot interaction energy; tunneling interactions[27–35] between dots are ignored.

Classical charging simulations of our experiments appear in Fig. 7, which shows the simulated double-dot conductance $\tilde{G}_{\rm dd}$ for identical dots as interdot capacitance $C_{\rm int}$ increases. The figure shows that classical charging can qualitatively reproduce the observed peak splitting.[13] However, quantitative agreement with experiment requires interdot capacitances $C_{\rm int}$ that increase strongly, unlike the classical capacitance for our geometry,[46] to a value $C_{\rm int}\sim 5$ fF that is over ten times greater than the *total* capacitance C_Σ measured for single dots. Furthermore the tunnel conductance is assumed to be negligible, while the actual measured tunnel conductance is $\sim e^2/h$. For similar reasons, the reported strong increase in effective dot-to-lead capacitance of single dots as the quantum point contacts are opened[41] is most likely a quantum effect controlled by tunneling.[32–35]

For double dots with mismatched gate capacitances, we observe not only tunneling induced peak splitting but also quasiperiodicity arising from classical charging.[7,22,23,30] Figure 8 illustrates the conductance $G_{\rm dd}$ of the double dot of device A using intentionally mismatched gate capacitances C_{26} and C_{36}, both controlled by V_6. As in Fig. 5, conductance peaks split as interdot tunnel conductance increases from Figs. 8(a)–8(d). Additional phenomena arising from unequal gate capacitance are also evident. Figure 8(a) demonstrates the stochastic Coulomb blockade,[7,22,23,30] in which conductance peaks become sparse at low temperatures for double dots with different gate capacitance and negligible interdot tunnel conductance. As shown in Figs. 8(b)–8(d),

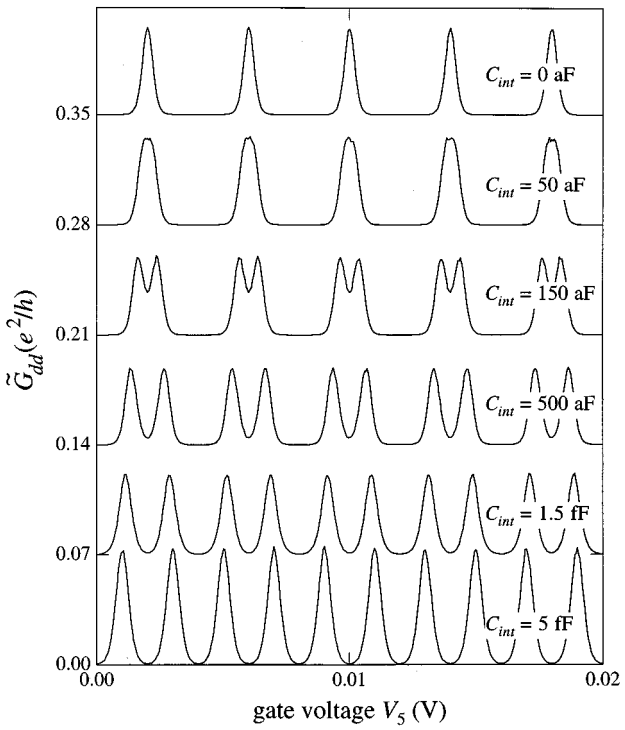

FIG. 7. Simulated double-dot conductance $\tilde{G}_{dd}$ vs gate voltage V_5 for increasing interdot capacitance C_{int} between identical dots. The classical charging model qualitatively resembles experiment, Fig. 5, but requires a negligible tunneling rate and unrealistically large interdot capacitance C_{int}, in contrast with experiment. From top to bottom, $C_{int}=0$ aF, 50 aF, 150 aF, 500 aF, 1.5 fF, and 5 fF. Curves are offset by $0.07e^2/h$ and use approximate experimental values as follows: total dot capacitance (excluding interdot capacitance) $C_\Sigma=480$ aF, gate capacitance $C_{25}=C_{35}=40$ aF, temperature $T=100$ mk, voltage bias $V_{bias}=10$ μV, and junction resistance $R=160$ kΩ.

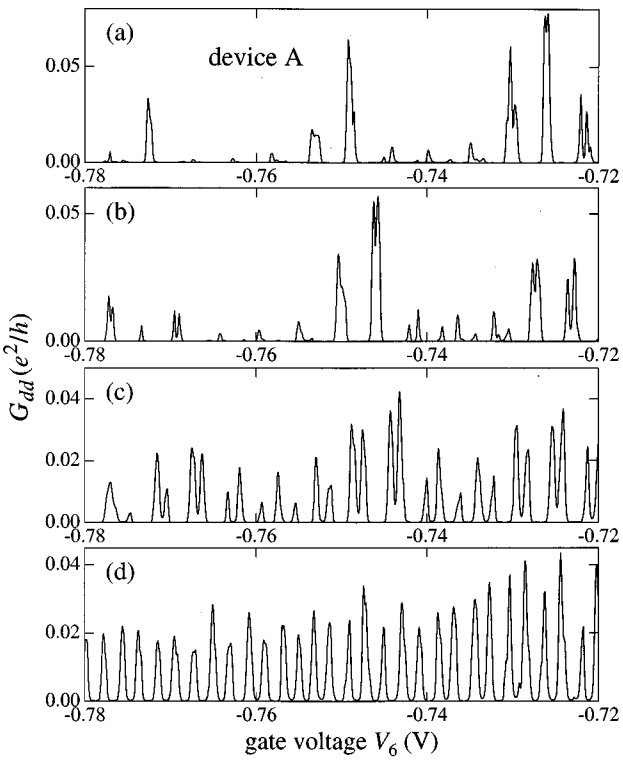

FIG. 8. For device A, double-dot conductance G_{dd} vs gate voltage V_6 as the interdot coupling increases from (a) to (d); the double dot is formed using dots 2 and 3. Gate capacitance mismatch causes peak suppression in (a) and quasiperiodicity in (c). The barrier conductance in units $2e^2/h$ is (a) 0.14, (b) 0.48, (c) 0.71, and (d) 0.95. The gate voltage V_3 controlling interdot tunnel barrier 3 is (a) -0.901 V, (b) -0.895 V, (c) -0.890 V, and (d) -0.880 V.

stronger interdot tunnel conductance lifts the stochastic Coulomb blockade, but capacitance mismatch is still apparent as quasiperiodic modulation of the peak amplitude and peak splitting.[30] This is in contrast to dots with nearly identical gate capacitances, shown in Fig. 5, for which the amplitude and splitting are more uniform. The measured beat period of $\sim$23 mV for Fig. 8(c) equals the period $e/|C_{36}-C_{26}|=23$ mV calculated with the gate capacitances measured for single dots. When the gate capacitances are more nearly matched, the beat period is longer and these phenomena become less prominent. For the top gates controlled by V_5, beating is sometimes observed with a period $\sim$70 mV, in good agreement with the expected period $e/|C_{35}-C_{25}|=80$ mV. No beating is observed for device B, for which the measured gate capacitances C_{14} and C_{24} are equal to within a few percent.

VI. TRIPLE QUANTUM DOTS

Peak splitting and quasiperiodicity are also observed for the triple dot formed by energizing all gates of device A. Conductance peaks split into three peaks when all gate capacitances are nealy equal, while complicated beating with a mix of single, double, and triple peaks occurs when gate capacitances are mismatched.

The measured change in triple-dot conductance G_{td} vs gate voltage V_5 as interdot tunnel conductance increases is plotted in Fig. 9, which is analogous to Fig. 5 for double dots. Weakly tunnel-coupled triple dots, Fig. 9(a), show conductance peaks with uniform spacing that is equal to the spacing for single dots in Fig. 4(a). As interdot tunnel conductance increases in Figs. 9(b) and 9(c), peaks split in two and in three; triply split peaks are more prevalent for stronger tunneling. The mismatch of gate capacitances C_{15}, C_{25}, and C_{35} is observable as an asymmetry of the split peaks. Finally, Fig. 9(d) shows the conductance when the tunnel barriers have been removed to create a single, large dot.

Figure 10 shows the triple-dot conductance G_{td} vs gate voltage V_6; this figure is analogous to Fig. 8 for double dots. As in Fig. 9, increased tunnel conductance causes peaks to split into double and triple peaks, with triple peaks prevalent for stronger tunneling. In addition, quasiperiodic beating appears due to the intentional mismatch of gate capacitance C_{26}; the observed beat period in Figs. 10(b) and 10(c) is $\sim$26 mV, agreeing well with the capacitances measured from single-dot data and with the double-dot beat period when gate voltage V_6 is swept. As for double dots, increasing tunnel conductance destroys the stochastic Coulomb blockade.

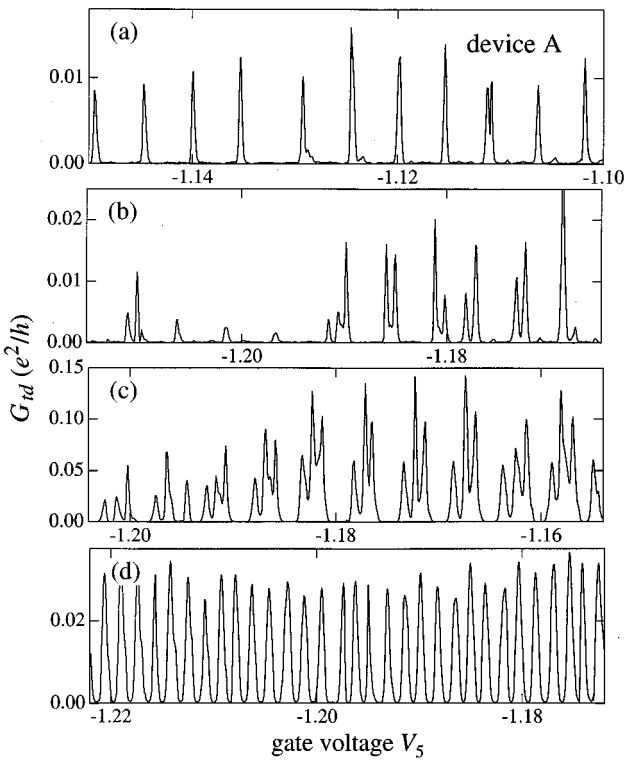

FIG. 9. For device A, triple-dot conductance G_{td} vs gate voltage V_5 as the interdot coupling increases from (a) to (d). Interdot coupling splits the conductance peaks into three peaks. Gate voltages V_2 and V_3, controlling interdot tunnel barriers 2 and 3, are (a) -0.839 V, -0.892 V; (b) -0.833 V, -0.887 V; (c) -0.828 V, -0.883 V; and (d) -0.795 V, -0.840 V.

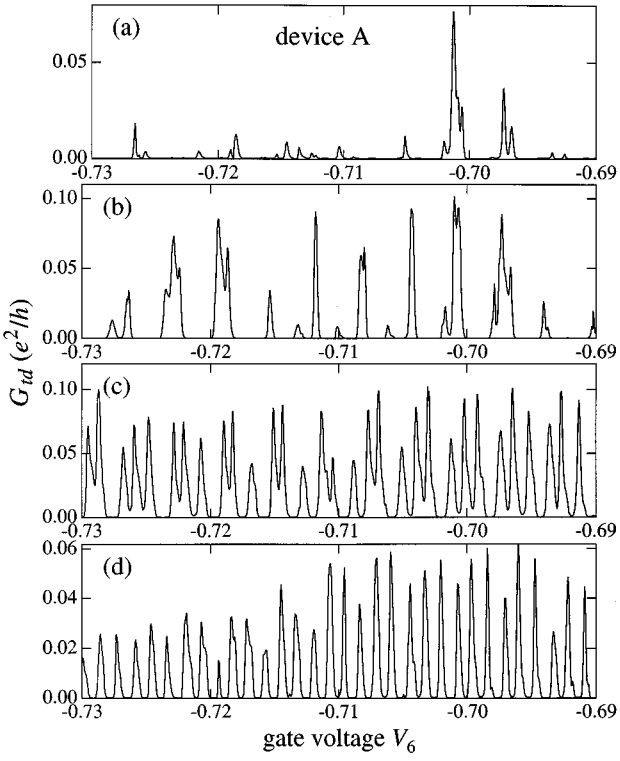

FIG. 10. For device A, triple-dot conductance G_{td} vs gate voltage V_6 as the interdot coupling increases from (a) to (d). The gate capacitance mismatch causes peak suppression in (a) and quasiperiodicity in (c). Gate voltages V_2 and V_3 controlling tunnel barriers 2 and 3, are (a) -0.835 V, -0.890 V; (b) -0.833 V, -0.888 V; (c) -0.823 V, -0.878 V, and (d) -0.784 V, -0.838 V.

Numerical simulations[13] of a classical charging model[20,22,23] for triple dots qualitatively resemble the data of Figs. 9 and 10, capturing both the splitting into triple peaks for identical dots and the complicated beating with single, double, and triple peaks for mismatched dots. However, as discussed in Sec. V for double dots, the simulations require unphysically large interdot capacitance and negligible interdot tunnel conductance, in contrast with experiment.

VII. SUMMARY

We have presented measurements of the tunnel conductance of double and triple quantum dots, showing that interdot tunneling leads to a variety of phenomena not observed in single dots. The most salient of these, conductance peak splitting controlled by interdot tunnel conductance, occurs when interdot tunneling lowers the energy of polarized charge configurations relative to unpolarized ones. We have shown experimentally that interdot tunneling splits conductance peaks into two peaks for double dots, and into three peaks for triple dots. We have also shown how gate capacitance mismatch gives rise to additional quasiperiodic structure in the conductance vs gate voltage, and how increasing tunnel conductance eventually destroys this quasiperiodicity.

We have presented a variety of evidence that tunneling, not classical charging, is responsible for the observed change in splitting with barrier conductance. The conductance between strongly coupled dots approaches $2e^2/h$, so that a classical capacitive picture assuming negligible interdot tunnel conductance is inappropriate. Moreover, our data agree well with theoretical predictions[30,31] of a universal relationship $F(G_{\mathrm{int}})$ between splitting F and interdot tunnel conductance G_{int} with limiting forms $F(0)\rightarrow 0$ for weak tunneling and $F(2e^2/h)\rightarrow 1$ for strong tunneling. Finally, numerical simulations of a capacitive charging model do not agree with experiment, requiring interdot capacitance to increase strongly, unlike the classical capacitance for our geometry, to unphysically large values. For these reasons we believe that quantum charge fluctuations due to interdot tunneling dominate dot interactions as the interdot conductance approaches $2e^2/h$.

ACKNOWLEDGMENTS

We thank B. I. Halperin and J. Golden for helpful discussions, and A. Adourian, J. Baskey, J. Hergenrother, J. Katine, D. Ralph, and S. Yang for experimental assistance. This research was supported at Harvard by the ONR under Grant Nos. N00014-95-1-0104 and N00014-95-1-0886, by the NSF under Grant No. DMR-91-19386, and by ARPA under Grant No. AFOSR-F49620-92-J-0466, and at UCSB by AFOSR-91-0214.

*Present address: Department of Physics 0319, University of California at San Diego, 9500 Gilman Drive, La Jolla, CA 92093-0319.

†Present address: Department of Biology, Harvard University, Cambridge, MA 02138.

‡Present address: Code 6341, Naval Research Laboratory, Washington, D.C. 20375.

[1] C. W. J. Beenakker and H. van Houten, in *Solid State Physics*, edited by H. Ehrenreich and D. Turnbull (Academic, San Diego, 1991), Vol. 44, p. 1, and references therein.

[2] M. A. Kastner, Rev. Mod. Phys. **64**, 849 (1992), and references therein.

[3] *Single Charge Tunneling*, edited by H. Grabert and M. H. Devoret (Plenum, New York, 1992), and references therein.

[4] D. V. Averin and K. K. Likharev, in *Mesoscopic Phenomena in Solids*, edited B. L. Altshuler, P. A. Lee, and R. A. Webb (North-Holland, Amsterdam, 1991), p. 173.

[5] L. P. Kouwenhoven, F. W. J. Hekking, B. J. van Wees, and C. J. P. M. Harmans, Phys. Rev. Lett. **65**, 361 (1990).

[6] R. J. Haug, J. M. Hong, and K. Y. Lee, Surf. Sci. **263**, 415 (1992).

[7] M. Kemerink and L. W. Molenkamp, Appl. Phys. Lett. **65**, 1012 (1994).

[8] T. Sakamoto, S. W. Hwang, F. Nihey, Y. Nakamura, and K. Nakamura, Jpn. J. Appl. Phys. **33**, 4876 (1994).

[9] F. Hofmann, T. Heinzel, D. A. Wharam, J. P. Kotthaus, G. Böhm, W. Klein, G. Tränkle, and G. Weimann, Phys. Rev. B **51**, 13 872 (1995).

[10] N. C. van der Vaart, S. F. Godijn, Y. V. Nazarov, C. J. P. M. Harmans, J. E. Mooij, L. W. Molenkamp, and C. T. Foxon, Phys. Rev. Lett. **74**, 4702 (1995).

[11] C. I. Duruöz, R. M. Clarke, C. M. Marcus, and J. S. Harris, Jr., Phys. Rev. Lett. **74**, 3237 (1995).

[12] F. R. Waugh, M. J. Berry, D. J. Mar, R. M. Westervelt, K. L. Campman, and A. C. Gossard, Phys. Rev. Lett. **75**, 705 (1995).

[13] F. R. Waugh, Ph.D. thesis, Harvard University, 1994.

[14] C. H. Crouch, C. Livermore, F. R. Waugh, R. M. Westervelt, K. L. Campman, and A. C. Gossard, Surf. Sci. (to be published).

[15] J. R. Tucker, J. Appl. Phys. **72**, 4399 (1992).

[16] C. S. Lent, P. D. Tougaw, and W. Porod, Appl. Phys. Lett. **62**, 714 (1993).

[17] P. D. Tougaw, C. S. Lent, and W. Porod, J. Appl. Phys. **74**, 3558 (1993).

[18] J. M. Martinis, M. Nahum, and H. D. Jensen, Phys. Rev. Lett. **72**, 904 (1994).

[19] P. D. Dresselhaus, L. Ji, S. Han, J. E. Lukens, and K. K. Likharev, Phys. Rev. Lett. **72**, 3226 (1994).

[20] N. S. Bakhvalov, G. S. Kazacha, K. K. Likharev, and S. I. Serdyukova, Zh. Eksp. Teor. Fiz. **95**, 1010 (1989) [Sov. Phys. JETP **68**, 581 (1989)].

[21] E. Castaño, G. Kirczenow, and S. E. Ulloa, Phys. Rev. B **42**, 3753 (1990).

[22] L. I. Glazman and V. Chandrasekhar, Europhys. Lett. **19**, 623 (1992).

[23] I. M. Ruzin, V. Chandrasekhar, E. I. Levin, and L. I. Glazman, Phys. Rev. B **45**, 13 469 (1992).

[24] C. Y. Fong, J. S. Nelson, L. A. Hemstreet, R. F. Gallup, L. L. Chang, and L. Esaki, Phys. Rev. B **46**, 9538 (1992).

[25] G. W. Bryant, Phys. Rev. B **48**, 8024 (1993).

[26] A. A. Middleton and N. S. Wingreen, Phys. Rev. Lett. **71**, 3198 (1993).

[27] C. A. Stafford and S. Das Sarma, Phys. Rev. Lett. **72**, 3590 (1994).

[28] G. Klimeck, Guanlong Chen, and S. Datta, Phys. Rev. B **50**, 2316 (1994).

[29] Guanlong Chen, G. Klimeck, S. Datta, Guanhua Chen, and W. A. Goddard III, Phys. Rev. B **50**, 8035 (1994).

[30] K. A. Matveev, L. I. Glazman, and H. U. Baranger (unpublished).

[31] J. M. Golden and B. I. Halperin (unpublished).

[32] G. Falci, G. Schön, and G. T. Zimanyi, Physica B **203**, 409 (1994).

[33] H. Schoeller and G. Schön, Phys. Rev. B **50**, 18 436 (1994).

[34] K. A. Matveev, Phys Rev. B **51**, 1743 (1995).

[35] G. Falci, G. Schön, and G. T. Zimanyi, Phys. Rev. Lett. **74**, 3257 (1995).

[36] J. A. Katine, M. J. Berry, R. M. Westervelt, and A. C. Gossard, Superlatt. Microstruct. **16**, 211 (1994).

[37] J. M. Martinis and M. Nahum, Phys. Rev. B **48**, 18 316 (1993).

[38] J. M. Hergenrother, J. G. Lu, M. T. Tuominen, D. C. Ralph, and M. Tinkham, Phys. Rev. B **51**, 9407 (1995).

[39] J. A. Nixon, J. H. Davies, and H. U. Baranger, Phys. Rev. B **43** 12 638 (1991).

[40] G. Timp, in *Physics of Nanostructures*, edited by J. H. Davies and A. R. Long (Institute of Physics, Philadelphia, 1992), p. 101.

[41] E. B. Foxman, P. L. McEuen, U. Meirav, N. S. Wingreen, Y. Meir, P. A. Belk, N. R. Belk, and M. A. Kastner, Phys. Rev. B **47**, 10 020 (1993).

[42] C. W. J. Beenakker, Phys. Rev. B **44**, 1646 (1991).

[43] V. Chandrasekhar and R. A. Webb, Phys. Rev. Lett. **67**, 2862 (1991).

[44] A. A. M. Staring, H. van Houten, and C. W. J. Beenakker, Phys. Rev. B **45**, 9222 (1992).

[45] S. W. Hwang, D. C. Tsui, and M. Shayegan, Phys. Rev. B **49**, 16 441 (1994).

[46] The capacitance per unit length between two thin coplanar rectangular metal strips of width ω and separation d in a medium with dielectric constant ε is $C/L=(2\varepsilon/\pi)\ln(2\omega/d)$ for $L\gg d$; for coplanar circular dots, curved facing edges cut off the log divergence, and the interdot capacitance varies slowly with d.